WATER RESOURCES RESEARCH, VOL. 31, NO. 11, PAGES 2743–2749, NOVEMBER 1995

Analysis of land surface heat fluxes using the orthonormal wavelet approach

Gabriel G. Katul[1] and Marc B. Parlange[2]
Hydrologic Science, University of California, Davis

Abstract. Heat fluxes under unstable atmospheric conditions are measured and analyzed using orthonormal wavelet expansions. Both wavelet and Fourier power spectra display a -1 power law that can be derived from dimensional arguments for latent and sensible heat flux in the turbulent production subrange. The wavelet expansion is used to investigate the spatial structure of the heat fluxes for those scales that exhibit a -1 power law. Dimensionless statistical measures which provide spatial information at different scales are developed and applied to the sensible and latent heat flux measurements. Deviations from Gaussian statistics were observed at the turbulent production subrange. The large flux events (both positive and negative) in the heat flux signals contribute directly to the energy and spatial structure of the -1 power law. The wavelet transform is used to identify the scale of turbulent action directly responsible for the tails observed in the horizontal gradient probability density function of both heat fluxes.

1. Introduction

To describe the turbulent transport mechanisms of latent heat (L_vE) and sensible heat (H) fluxes into the atmosphere it is important to characterize the properties of the energy-containing eddies. It is well recognized that the turbulent eddies in the atmosphere are intermittent, local, and nonperiodic and produce large fluctuations [*Gao et al.*, 1989]. At any instant in time the heat fluxes can be decomposed as

$$\begin{aligned} L_v w'q' &= L_v\langle w'q'\rangle + L_vE' \\ \rho C_p w'T' &= \rho C_p\langle w'T'\rangle + H' \end{aligned} \tag{1}$$

where w', T', and q', are the turbulent fluctuations of the vertical velocity, temperature, and vapor density, respectively, angle brackets denote the time-averaging operation, L_v is the latent heat of vaporization, ρ is the air density, c_p is the specific heat capacity, and H' and L_vE' are fluctuations about the time averages. The fluctuations H' and L_vE' display extreme variability and can be orders of magnitude larger than the mean turbulent flux. Improved understanding of flux variability is useful for better parameterization of sensible and latent heat fluxes from the land surface.

The objectives of this study are (1) to quantify spatial properties of H' and L_vE' at different scales using wavelet transforms and (2) to examine possible dynamical (local and global) similarities between H' and L_vE' using direct field measurements.

To quantify space-scale relations, a representation that decomposes turbulent flux measurements into contributions of different scales as well as different locations is needed. This representation requires basis functions that behave like localized pulses rather than extended waves (e.g., Fourier kernel). If additional requirements such as self-similarity are imposed, specific basis functions, known as wavelets, are then generated. Thus wavelet transforms are well suited for the first objective.

In the second objective, global similarity is defined in terms of the entire measured flux time series with no attention paid to particular events. By local similarity we mean similarity of specific local events, for example, large flux changes over short time periods. In this study, measurements of vertical velocity, temperature, and vapor density at 80 cm above a uniform bare soil surface are analyzed. These measurements permit a direct estimate of H' and L_vE' in time (which can be converted to space using Taylor's hypothesis).

2. Wavelet Transforms

Wavelet transforms are recent mathematical tools based on group theory of square integrable functions (i.e., functions with finite variance) that decompose signals, functions, or operators into space and scale. Wavelet transforms are classified under two broad categories: (1) continuous wavelet transforms, and (2) discrete wavelet transforms [*Chui*, 1992, pp. 13–22]. *Daubechies* [1992, p. 7] further classifies the discrete wavelet transforms as (1) redundant discrete systems (also known as frames), and (2) orthonormal wavelet expansions. In the following section, continuous wavelet transforms are introduced, and a description of orthonormal wavelet expansions is given.

2.1. Continuous Wavelet Transforms

Continuous wavelet transforms were introduced by *Grossmann and Morlet* [1984, 1985] and have been applied to various turbulence measurements [*Argoul et al.*, 1989; *Liandrat and Moret-Bailly*, 1990; *Everson et al.*, 1990; *Barcy et al.*, 1991; *Farge*, 1992b]. These studies demonstrate the usefulness of continuous wavelet transforms in detecting singularities and fractal structure in turbulence measurements.

The continuous wavelet transform of a real square integrable function $f(x)$ with respect to a real integrable analyzing wavelet $\psi(x)$ may be defined as

[1]Now at School of the Environment, Duke University, Durham, North Carolina.
[2]Also at Biological and Agricultural Engineering, University of California, Davis.

Paper number 95WR00003.
0043-1397/95/95WR-00003$05.00

$$W(b, a) = C_g^{-1/2} \frac{1}{a^{1/2}} \int_{-\infty}^{+\infty} \psi\left(\frac{t-b}{a}\right) f(t)\, dt \qquad (2)$$

where a is a scale dilation, b is a position translation, and C_g is defined by

$$C_g = \int_{-\infty}^{+\infty} |k|^{-1} |\psi^*(k)|^2\, dk < \infty \qquad (3)$$

Here k is the wavenumber and ψ^* is the Fourier transform of $\psi(x)$ given by

$$\psi^*(k) = \int_{-\infty}^{+\infty} \psi(y) e^{-iky}\, dy. \qquad (4)$$

The function $\psi(x)$ is an analyzing wavelet if it satisfies the following three conditions [*Farge*, 1992a; *Grossmann et al.*, 1989]: (1) The admissibility condition, which requires that

$$\int_{-\infty}^{+\infty} \psi(y)\, dy = 0 \qquad (5)$$

(2) the similarity condition, which requires the scale decomposition to be obtained by translation and dilation of one unique function $\psi(x)$ [*Farge*, 1992a], and (3) the invertibility condition, which requires at least one reconstruction formula for recovering the signal from its wavelet coefficients. The function $f(x)$ may be recovered from the wavelet coefficients by

$$f(x) = C_g^{-1/2} \int_0^{+\infty} \int_{-\infty}^{+\infty} a^{-1/2} \psi\left(\frac{x-b}{a}\right) W(a, b) \frac{dx\, da}{a^2}. \qquad (6)$$

Further details regarding continuous wavelet transforms can be found in many references [e.g., *David*, 1992; *Chui*, 1992]. *Yamada and Ohkitani* [1990, 1991a, b] showed that continuous wavelets are not very effective in investigating energy aspects of turbulence because the kernel functions are not mutually orthogonal. The nonorthogonality brings about formal relations between the wavelet coefficients, and hence no immediate physical interpretation can be associated with the wavelet coefficients [*Yamada and Ohkitani*, 1990, 1991a, b].

2.2. Orthonormal Wavelet Expansions

Some of the material presented in this section is also discussed by *Katul and Parlange* [1994]. For completeness we present the main points and key results. For actual turbulence measurements, discrete wavelet transforms are preferable since $f(x)$ is generally known at only discrete points x_j. This requires the discretization of (2) in the scale and space domain. The discretization of the domain of (2) is not arbitrary since conservation of the amount of information in the signal is necessary. As shown by *Daubechies* [1988, 1992, p. 10] and *Mallat* [1989a, b], using a logarithmic uniform spacing for the scale discretization with increasingly coarser spatial resolution at larger scale, a complete orthogonal wavelet basis can be constructed with

$$\psi_{[j]}^{(m)}(y) = a_0^{-m/2} \psi\left(\frac{y - j b_0 a_0^m}{a_0^m}\right) \qquad (7)$$

where m and j are variable scale and position indices, respectively, a_0 is the base of the dilation, b_0 is the translation length in units of a_0^m, and (m) is used as a scale index (not to be confused with power m). The simplest and most efficient case for practical computation is the dyadic arrangement resulting in $a_0 = 2$ and $b_0 = 1$ [*Daubechies*, 1992, p. 10; *Chui*, 1992, p. 4; *Mallat*, 1989a, b; *Meyer*, 1989]. All scales along octaves 2^m and translations along $2^m j$ contribute to the construction of $f(x_j) = f(j)$ using

$$f(j) = \sum_{m=1}^{m=\infty} \sum_{i=-\infty}^{i=+\infty} W^{(m)}[i] g^{(m)}[i - 2^m j] \qquad (8)$$

where $g^{(m)}[i]$ is the discrete version of the wavelet function $\psi(x)$ at scale m. Notice how the translations are dependent on the dilations. The discrete wavelet function $g^{(m)}[i]$ satisfies the orthogonality condition

$$\sum_{k=-\infty}^{k=+\infty} g^{(m)}[k - 2^m j] g^{(n)}[k - 2^n j] = \delta_{ij} \delta_{mn} \qquad (9)$$

where δ_{ij} is the Kronecker delta function. The discrete wavelet coefficients at scale index m and position index i can be computed by

$$W^{(m)}[i] = \sum_{i=-\infty}^{i=+\infty} g^{(m)}[i - 2^m j] f(j) \qquad (10)$$

and they satisfy the conservation of energy condition

$$\sum_{j=-\infty}^{j=+\infty} f(j)^2 = \sum_{m=1}^{m=+\infty} \sum_{i=-\infty}^{i=+\infty} (W^{(m)}[i])^2. \qquad (11)$$

Notice that this is similar to Parseval's identity in Fourier series

$$\frac{1}{2\pi} \int_0^{2\pi} |f(x)|^2\, dx = \sum_{n=-\infty}^{n=+\infty} |c_n|^2 \qquad (12)$$

where c_n are the Fourier coefficients defined by

$$c_n = \frac{1}{2\pi} \int_0^{2\pi} f(x) e^{-inx}\, dx \qquad (13)$$

In practice, the number of heat flux measurements are finite, and the summations in the above equations do not extend to infinity. To modify the above equations for a finite number of observations, let $N = 2^M$ be the number of observations (i.e., N is an integer power of 2). The scale index m then varies from 1 to $M = \log_2(N)$, and the position index at scale m varies from 1 to $N \times 2^{-m}$. Note that this definition implies that as the scale increases, the spatial resolution becomes much coarser (e.g., at $m = 1$, we have $N/2$ coefficients, at $m = 2$ we have $N/4$ coefficients, at $m = M$ we have 1 coefficient). Note also that the above arrangement conserves the number of wavelet coefficients ($=N - 1$) required to decompose the turbulence signal defined over N points. This dyadic arrangement is well suited for turbulence studies, since the small-scale features of the turbulence signal, which change rapidly compared to the large-scale features, are characterized by more wavelet coefficients. A simple procedure to determine the wavelet coefficients is discussed next.

2.3. Determination of the Wavelet Coefficients

Following *Mahrt* [1991], the *Haar* [1910] wavelet is well suited for capturing rapid changes in turbulence signals due to its locality in physical space. Since locality in physical space is critical for the present study, we choose the Haar basis as our analyzing wavelet. The Haar basis $\psi(x) = (a^{-1/2})\psi[(x - b)/a]$, where $a = 2^m$ and $b = 2^m i$ for $i, m \in Z$, is given by

$$\psi(x) = 1 \qquad 0 \le x < \tfrac{1}{2}$$

$$\psi(x) = -1 \qquad \tfrac{1}{2} \le x < 1 \tag{14}$$

$$\psi(x) = 0 \qquad \text{elsewhere}$$

As shown by *Beylkin et al.* [1991, 1992], for this basis function the wavelet coefficients $W^{(m+1)}(k)$ and the coarse-grained signal $S^{(m+1)}(k)$ at scale $m + 1$ can be determined from the signal $S^{(m)}$ at scale m by using

$$W^{(m+1)}(i) = \frac{1}{2^{1/2}}[S^{(m)}(2i - 1) - S^{(m)}(2i)] \tag{15}$$

$$S^{(j+1)}(k) = \frac{1}{2^{1/2}}[S^{(j)}(2k - 1) + S^{(j)}(2k)] \tag{16}$$

for $m = 0$ to $M - 1$, $i = 0$ to $2^{M-m-1} - 1$, and $M = \log_2(N)$, N is the number of samples (integer power of 2). For the Haar wavelet, $S^{(m+1)}$ is a low-pass filtered function obtained by a simple block moving average. The wavelet coefficients and coarse-grained signal may be calculated by the following pyramidal algorithm discussed by *Katul and Parlange* [1994]:

1. Beginning with $m = 0$, use (9) and (10) to calculate the signal $S^{(1)}$ and the coefficients $W^{(1)}$ at the first scale by looping over i from 0 to $2^{M-1} - 1$. This will result in S and W vectors of length $N/2$.
2. Repeat step 1 with $m = 1$ to calculate the next coarser scale's pair of vectors S^2 and W^2 (each of length $N/4$).
3. Repeat for larger scale m up to $M - 1$ to produce a series of S and W vectors of progressively decreasing length. Note that at $m = M - 1$ the coarse-grained signal converges to a point.

This algorithm yields $N - 1$ Haar wavelet coefficients that define the orthonormal wavelet transform of the measured heat flux signal. The above pyramidal procedure constitutes the basis for fast wavelet transforms (FWT) and requires about N computations in comparison to the $N \log_2 N$ computations for fast Fourier transforms (FFT). Recall from (11) that the $N - 1$ discrete Haar wavelet coefficients satisfy the conservation of energy condition.

3. Experimental Setup

Measurements of H and L_vE were carried out at the University of California, Davis, Campbell Tract research site (elevation above sea level, 18 m), which extends some 500 m × 500 m. These measurements were made in the atmospheric surface layer above a uniform bare soil field with a momentum roughness height (z_0) of 2 mm. Further details on the field site are presented by *Katul and Parlange* [1992] and *Parlange and Katul* [1992]. A Campbell Scientific one-dimensional sonic anemometer (model CA27; sonic path length, 15 cm), an ultraviolet krypton hygrometer (model KH20; path length, 1.105 cm), and a fine wire chromel constantan thermocouple (thickness, 0.0127 mm) were positioned at 80 cm above the ground surface to measure w', q', and T', respectively. The fine wire thermocouple measures the difference between the air temperature and a large time-constant (1 hour) temperature probe, which is inside the CA27 base mount. The resolution of the thermocouple is 0.005°C. The krypton hygrometer (model KH20) measures the absolute vapor density in the air with a resolution of 0.031 g m^{-3}. Details regarding the theory of operation of these sensors may be found in the works by *Friehe* [1986], *Kaimal* [1986], and *Tanner* [1988]. The instruments were logged at 10 Hz using a 21X Campbell Scientific micrologger, and the data were transferred to a Hi-level Chrome (70 μs) tape every 5 s. The experiment was carried out on day of year 280 in 1992 (at 2:32 p.m.). The sampling duration for the experiment was 27.3 min (i.e., $N = 16{,}384$ data points). The mean wind speed $\langle U \rangle$ was 1.7 m s^{-1}. Note that the combination of $f = 10$ Hz, $\langle U \rangle = 1.7$ m s^{-1}, and $z = 80$ cm satisfies the dimensionless frequency ($fz/\langle U \rangle$) criteria proposed by *Kaimal et al.* [1972], *McBean* [1972], and *Monin and Yaglom* [1975, pp. 456–457] for adequately resolving wavenumbers responsible for scalar transport given by

$$10^{-3} < (fz/\langle U \rangle) = 4.71 < 10. \tag{17}$$

In addition, since the turbulent intensity ($u'/\langle U \rangle$) was less than 0.5, *Taylor*'s [1938] hypothesis can be used to convert time measurements to space measurements [*Lumley*, 1965; *Powell and Elderkin*, 1974; *Willis and Deardorff*, 1976; *Wyngaard and Clifford*, 1977]. A summary of the meteorological conditions is presented in Table 1.

Table 1. Summary of Meteorological Conditions During Study

Parameter	Value
Day of year (1992)	280
Local time	1332
u_*, m s^{-1}	0.217
H, W m^{-2}	173.18
LE, W m^{-2}	35.4
T_a, °C	31.8
RH, %	9.95
R_n, W m^{-2}	346.1
G, W m^{-2}	114.1
Obukhov length, m	−5.8

The friction velocity (u_*) was estimated from a Young triaxial propeller anemometer, the mean air temperature (T_a) and mean air relative humidity (RH) were measured at 80 cm using a Phys-Chem nonlinear thermistor and humidity transducers, the net radiation (R_n) was measured by a Fritshen type total hemispherical sensor, and the soil heat flux (G) was measured by a Thornwaite soil heat flux plate placed at 0.3 cm below the ground surface. The Obukhov length ($= -\rho u^3 [kg(H/c_pT_a + 0.61 L_vE/L_v)]^{-1}$) is also displayed, where $k = 0.4$ is the von Kármán constant, $g = 9.81$ m s^{-2} is the gravitational acceleration, and $c_p = 1005$ J kg^{-1} K^{-1} is the specific heat capacity of dry air.

4. Spatial Statistics of Heat Fluxes

In this section we introduce statistical tools that utilize wavelet coefficients for characterizing the spatial variation of "energy" of the measured heat fluxes. In this study "energy" is considered to be the variance of the heat fluxes.

4.1. Wavelet Spectra

The variance of a signal, in terms of the wavelet coefficients, can be deduced from (11),

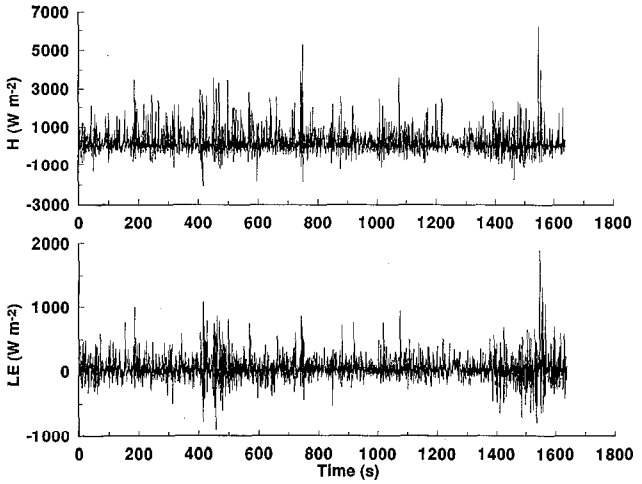

Figure 1. Time series (10 Hz) of sensible ($\rho c_p w'T'$) and latent ($L_v w'q'$) heat flux measurements for unstable stability conditions.

$$\sigma^2 = N^{-1} \sum_{m=1}^{m=M} \sum_{i=1}^{i=N} (W^{(m)}[i])^2 \tag{18}$$

where N is the number of observations (power of 2), M is $\log_2(N)$, m is the scale index, and i is the position index. The total energy T_E contained in scale $R_m = (2^m dy)$ is given by

$$T_E = N^{-1} \sum_{i=1}^{i=2^{M-m}} (W^{(m)}[i])^2. \tag{19}$$

For comparing the wavelet and Fourier power spectra, we define a wavenumber corresponding to scale R_m as

$$k_m = 2\pi/R_m. \tag{20}$$

The power spectral density function, defined as the total energy per unit wavenumber, is obtained at wavenumber k_m by dividing (19) with $\Delta k_m = (2\pi)2^{-m}(dy)^{-1} \ln(2)$ to give

$$E(k_m) = \langle (W^{(m)}[i])^2 \rangle \frac{dy}{2\pi \ln(2)} \tag{21}$$

where angle brackets denote the space average over all values of i. Notice that the wavelet power spectrum is obtained by averaging many squared wavelet coefficients in space at each wavenumber. The standard deviation for this spatially averaged energy at wavenumber k_m can be computed from the wavelet coefficients using

$$\mathrm{SD}_E(k_m) = \frac{dy}{2\pi \ln(2)} [\langle (W^{(m)}[i])^4 \rangle - \langle (W^{(m)}[i])^2 \rangle^2]^{1/2}. \tag{22}$$

A plot of $E(k_m)$ and $E(k_m) + \mathrm{SD}_E(k_m)$ gives a compact representation of the energy and a measure of its spatial variability at each scale. This type of representation is known as the "dual spectrum" [*Meneveau*, 1991a, b]. Another useful measure of the spatial variation of energy is the coefficient of variation (CV) defined by

$$\mathrm{CV}(K_m) = \mathrm{SD}(K_m)/E(K_m) \tag{23}$$

Notice the difference between the wavelet and the Fourier energy spectra. Due to the global nature of Fourier transforms, the energy at each wavenumber is distributed uniformly in space so that $\mathrm{SD}_E = 0$. However, depending on the variability of the energy in space, wavelet transforms generally exhibit a positive SD_E.

4.2. Spatial Statistics of Turbulence

The wavelet skewness $\mathrm{SF}(k_m)$ and the wavelet flatness factors $\mathrm{FF}(k_m)$,

$$\mathrm{SK}(k_m) = \langle (W^{(m)}[i])^3 \rangle / \langle (W^{(m)}[i])^2 \rangle^{3/2} \tag{24}$$

$$\mathrm{FF}(k_m) = \langle (W^{(m)}[i])^4 \rangle / \langle (W^{(m)}[i])^2 \rangle^{4/2} \tag{25}$$

can be computed at each scale k_m. These dimensionless factors are used to characterize the spatial statistics (e.g., deviations from Gaussian properties) of the wavelet coefficients.

The wavelet transform amplifies the changes in the flux signal rather than the absolute magnitude of the flux events. This is important for the identification of sharp changes in the flux measurements. The wavelet skewness and wavelet flatness factors are also statistical measures of the horizontal gradients in the flux signal since converting a difference to a gradient simply requires the division by a characteristic scale. This characteristic scale cancels out in both ratios of (24) and (25). Hence the wavelet skewness is a dimensionless measure of the magnitude and the sign of the preferred direction of the horizontal gradients, while the wavelet flatness factor measures the importance of large spatial gradients in the flux signal at scales k_m. These spatial differences in the flux signal arise due to rapid transient turbulent motion that simultaneously changes the scalar as well as the vertical velocity fluctuations. Finally, the wavelet flatness factor defined in (25) differs from the conventional central moment flatness factor. The central moment flatness factor measures the importance of extreme flux events in relation to the mean flux (i.e., sensitive to the magnitude of flux events), while the wavelet flatness factor measures the importance of rapid changes in the flux measurements.

5. Results and Discussion

The time series of the sensible and latent heat fluxes are presented in Figure 1. Notice that the fluctuations about the mean flux can be 1 or 2 (in the case of $L_v E$) orders of magnitude larger than the mean flux. The integral timescales of both fluxes are 0.5 s, which is smaller than the individual integral timescales of w', T', and q' (see Table 2). The similarity between the flux integral timescales suggests some similarity between H' and $L_v E'$ at production scales.

Table 2. Integral Timescale Summary

Variable	Timescale, s	Length Scale, m
w'	1.1	1.87
T'	2.9	4.93
q'	3.9	6.63
$w'T'$	0.50	0.85
$w'q'$	0.50	0.85

The integral timescale was calculated from integrating the area under the autocorrelation function up to the first zero crossing. The integral timescales of the fluxes are also shown. Integral length scales are calculated from integral timescales using Taylor's hypothesis.

5.1. Wavelet Spectra

In Figure 2, a comparison between the Fourier power spectra and the Haar wavelet spectra for H' and $L_v E'$ is presented. The agreement between the wavelet spectrum and the Fourier power spectrum is well within the scatter of the Fourier power spectra. The Fourier spectrum was computed by square windowing 2048 points, cosine tapering 5% each window side, and then averaging the eight resultant power spectra [*Press et al.*, 1990]. The wavelet power spectrum was computed by (1) using the pyramidal algorithm defined in (15) and (16) to obtain the Haar wavelet coefficients in space and scale and (2) using (25) in conjunction with the wavelet coefficients from step 1 to obtain the wavelet power spectrum at wavenumber k_m. Notice in Figure 2 that a -1 power law exists in the power spectra at the wavenumber ($=7.4\ \mathrm{m}^{-1}$) which corresponds to the integral length scale ($=0.85$ m) (see Table 2). The -1 power law in the flux spectra can be derived from similarity theory, which is considered next.

Following *Tennekes and Lumley* [1972], the dimensionless power spectrum for H' and $L_v E'$ at small wavenumbers can be written

$$\frac{E_{H'}}{(\rho c_p \langle w'T' \rangle)^2 z} = F_H(Kz) \qquad \frac{E_{L_v E'}}{(L_v \langle w'q' \rangle)^2 z} = F_{L_v E}(Kz) \tag{26}$$

where $F(\ )$ are universal functions that depend on the dimensionless wavenumber Kz. The application of (26) is restricted to wavenumbers for which viscosity is not important. These wavenumbers correspond to dynamically important scales that are comparable to the integral length scale. At these scales, variables affecting the mean flow become important. Using the height independent arguments proposed by *Kader and Yaglom* [1990, 1991] for E_H and $E_{L_v E}$ allows (26) to be written

$$\frac{E_{H'}}{(\rho c_p \langle w'T' \rangle)^2 z} = \frac{C_H}{(Kz)} \qquad \frac{E_{L_v E'}}{(L_v \langle w'q' \rangle)^2 z} = \frac{C_{L_v E}}{(Kz)} \tag{27}$$

so that the flux power spectra are proportional to K^{-1}, and C_H and $C_{L_v E}$ are universal constants. Using the spectra of Figure 2, we determined C_H and $C_{L_v E}$ to be 1.14 and 1.8, respectively.

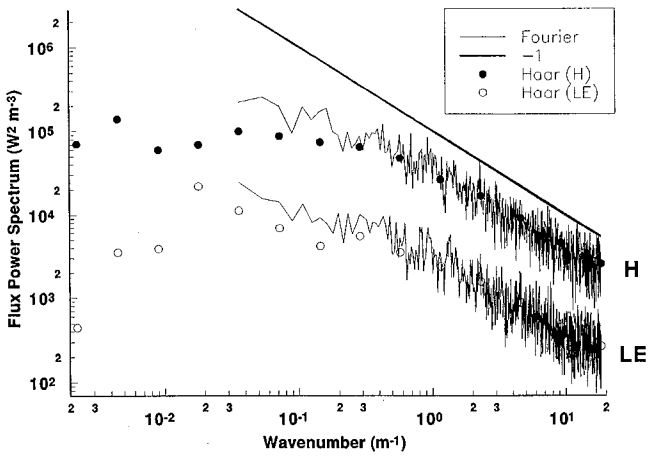

Figure 2. Comparison of Fourier (solid line) and wavelet (circles) power spectra for both heat fluxes. The -1 power law (thick line) is also shown.

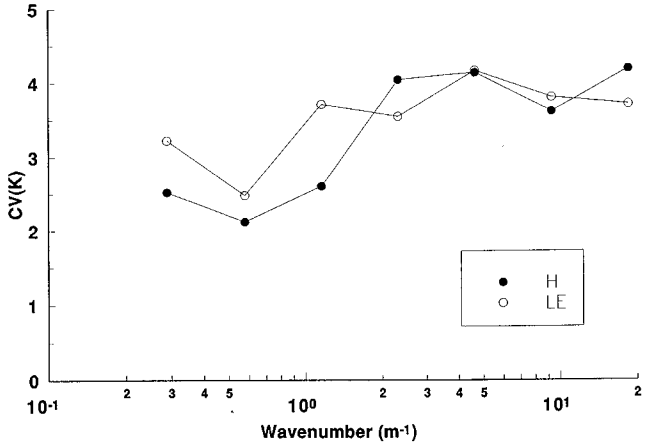

Figure 3. The coefficient of variation (CV) as a function of wavenumber for sensible and latent heat flux.

5.2. Spatial Statistics of Turbulence

In this section two aspects of the spatial statistics of the turbulent fluxes are presented: (1) energy (or flux variance) and (2) horizontal gradients. In Figure 3 the coefficient of variation (CV) is shown as a function of K_m for both latent and sensible heat fluxes. The coefficient of variation was computed (1) using the pyramidal algorithm defined by (15) and (16) to obtain the wavelet coefficient and (2) applying (23) to the coefficients obtained in step 1. Notice in Figure 3 that CV was larger than unity, indicating that the variability in the flux energy is much greater than the mean value. Also, CVs for H' and LE', within the -1 power law range, are very similar, while for other scales marked differences in CV are observed. Recall that CV involves the averaging of the fourth power of the wavelet coefficients at position index (i) for scale index (m). Hence CV is very sensitive to local events (at scale m) occurring in space. Similarity in CV between the flux signals indicates statistical similarity in local events at scale (m). Therefore this analysis indicates that local similarity between H' and LE' does hold (as was assumed in (26), (27), and (28)). This becomes more evident in Figure 4, in which the wavelet skewness and flatness factors for the sensible and latent heat fluxes are shown. The wavelet skewness and flatness factors were computed applying (23) and (24). Notice in Figure 4 that the wavelet flatness factor is much larger than 3, indicating strong non-Gaussian statistics in the flux signals (at least within the -1 power law range). These large flatness factors in both flux signals suggest that the tails of the probability density function (pdf) of the horizontal gradients extend beyond a Gaussian behavior. To illustrate this in Figure 5, we compare the pdf's of both heat flux gradients with a Gaussian pdf. The pdf in Figure 5 was computed by (1) applying Taylor's hypothesis to convert the time domain to a space domain, (2) approximating the gradient by differencing adjacent points in both heat flux signals, (3) normalizing the differenced signals to have a zero mean and unit variance, and (4) computing the frequency distribution of the normalized series using 200 bins (recall $N = 16{,}384$). The ordinate axis shown in Figure 5 is logarithmic in order to emphasize the behavior at the tails. Notice the similarity between the latent and sensible heat flux gradient pdf's, especially at the tails.

The eddy sizes contributing to the tails of the pdf's in Figure 5 can be estimated using the wavelet skewness and flatness

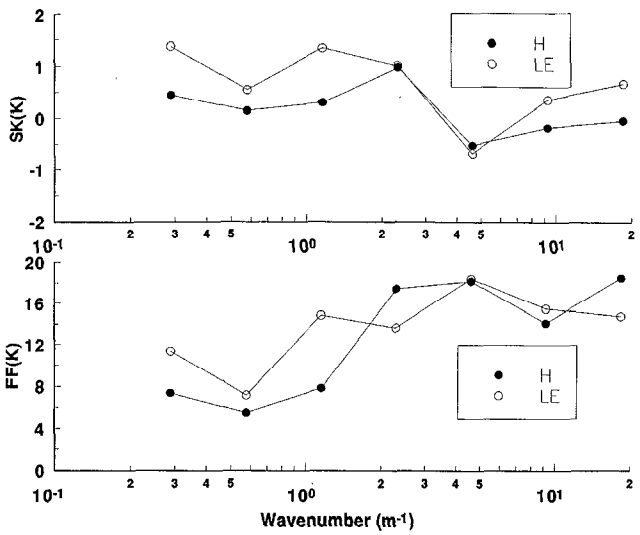

Figure 4. Wavelet skewness (SK) and flatness factors (FF) as a function of wavenumber K for sensible and latent heat flux.

factors (see Figure 4). The largest wavelet flatness factor corresponds to wavenumbers within the -1 production subrange where most negative wavelet skewness occurs (see Figure 4). This suggests that these scales contribute most to the tails in Figure 5.

6. Conclusions

The usefulness of orthonormal wavelet expansions in analyzing the spatial structure of atmospheric surface layer heat fluxes is examined. The advantage of wavelet decomposition is its capability of decomposing the heat flux into "flow independent wavelets" for various wavenumbers and positions. By flow independent wavelets we mean that a wavelet basis is selected that is independent of the flow dynamics.

It was found that the latent and sensible flux Fourier and wavelet spectra exhibit a -1 power law at wavenumbers comparable to the integral length scales. The -1 power law in both fluxes was derived using dimensional arguments. These arguments are based on similarity between the latent and sensible heat flux fluctuations about the mean turbulent fluxes. Due to the spatial localization of the Haar basis, we considered the spatial statistics of the wavelet coefficients at wavenumbers corresponding to the -1 power law. We defined and utilized three space-scale statistical quantities: (1) the coefficient of energy variation, (2) the wavelet skewness, and (3) the wavelet flatness factor. It was found that these wavelet spatial statistics for sensible and latent heat fluxes were comparable over the -1 power law range. The fact that these statistics are comparable suggests a space-scale statistical similarity in local events for both fluxes. We utilized the wavelet skewness and flatness factors to identify the importance of localized events on the tails of the horizontal gradient probability density function of the fluxes. It was found that scales within the -1 power law range directly contribute to the widening of the tails of the gradient probability density function.

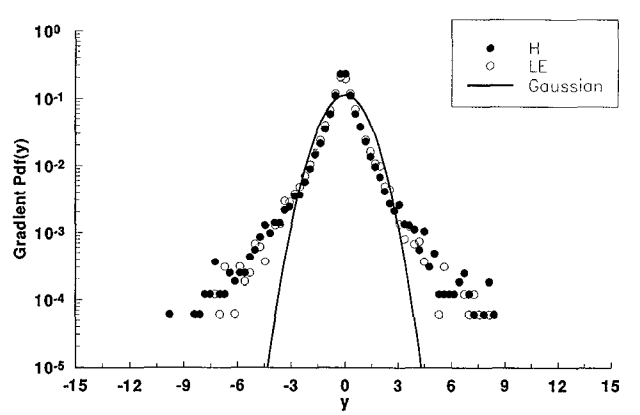

Figure 5. Horizontal gradient probability density function (pdf) for normalized heat fluxes (y). The normalized sensible and latent heat fluxes have zero mean and unit variance. The Gaussian pdf (solid line) is also shown.

Acknowledgments. The authors would like to thank Chia Ren Chu and John Albertson for helpful discussions, David Buscagli for his programming assistance, Mike Mata for his help in maintaining the field, and Roger Shaw and Larry Mahrt for helpful discussions. This work was supported in part by the National Science Foundation (EAR-93-04331), Kearney Foundation, Water Resources Center (W-812), USGS, and UC Davis superfund (5 P42ES04699-07).

References

Argoul, F., A. Arneodo, G. Grasseau, Y. Gagne, E. J. Hopfinger, and U. Frisch, Wavelet analysis of turbulence reveals the multifractal nature of the Richardson cascade, *Nature, 338*, 51–53, 1989.

Barcy, E., A. Arneodo, U. Frish, Y. Gagne, and E. Hopfinger, Wavelet analysis of fully developed turbulence data and measurement of scaling exponents, in *Turbulence and Coherent Structures*, edited by O. Metais and M. Lesieur, pp. 203–215, Kluwer Academic, Norwell, Mass., 1991.

Beylkin, G., R. Coifman, and V. Rokhlin, Fast wavelet transforms and numerical algorithms, I, *Commun. Pure Appl. Math., XLIV*, 141–183, 1991.

Beylkin, G., R. Coifman, and V. Rokhlin, Wavelets in numerical analysis, in *Wavelets and Their Applications*, edited by M. B. Ruskai, G. Beylkin, R. Coifman, I. Daubechies, S. Mallat, Y. Meyer, and L. Raphael, pp. 181–210, Jones and Bartlett, Boston, Mass., 1992.

Chui, C. K., *An Introduction to Wavelets*, 264 pp., Academic, San Diego, Calif., 1992.

Daubechies, I., Orthonormal bases of compactly supported wavelets, *Commun. Pure Appl. Math., XLI*, 909–996, 1988.

Daubechies, I., *Ten Lectures on Wavelets, CBMS-NSF Regional Conf. Ser. Appl. Math.*, vol. 61, 357 pp., Society for Industrial and Applied Mathematics, Philadelphia, Pa., 1992.

David, G., *Wavelets and Singular Integrals on Curved Surfaces*, 109 pp., Springer-Verlag, New York, 1992.

Everson, R., L. Sirovich, and K. R. Sreenivasan, Wavelet analysis of the turbulent jet, *Phys. Lett. A, 145*, 314–322, 1990.

Farge, M., Wavelet transforms and their applications to turbulence, *Annu. Rev. Fluid Mech., 24*, 395–457, 1992a.

Farge, M., The continuous wavelet transform of two dimensional turbulent flows, in *Wavelets and Their Applications*, edited by M. B. Ruskai, G. Beylkin, R. Coifman, I. Daubechies, S. Mallat, Y. Meyer, and L. Raphael, pp. 275–302, Jones and Bartlett, Boston, Mass., 1992b.

Friehe, C., Fine scale measurements of velocity, temperature, and humidity in the atmospheric boundary layer, in *Probing the Atmospheric Boundary Layer*, edited by D. H. Lenschow, pp. 29–38, American Meteorological Society, Boston, Mass., 1986.

Gao, W., R. H. Shaw, and K. T. Paw U, Observation of organized structure in turbulent flow within and above a forest canopy, *Boundary Layer Meteorol., 47*, 349–378, 1989.

Grossmann, A., and J. Morlet, Decomposition of Hardy functions into square integrable wavelets of constant shape, *SIAM J. Math. Anal., 15*, 723–736, 1984.

Grossmann, A., and J. Morlet, Decomposition of functions into wavelets of constant shape, and related transforms, *Mathematics + Phys-*

ics, Lectures on Recent Results, edited by L. Streit, World Scientific, Singapore, 1985.

Grossmann, A., R. Kronland-Martinet, and J. Morlet, Reading and understanding continuous wavelet transforms, in *Wavelets: Time-Frequency Methods and Phase Space*, edited by J. M. Combes, A. Grossmann, and P. Tchamitchian, pp. 2–20, Springer-Verlag, New York, 1989.

Haar, A., Zur Theorie der orthogonalen Funktionensysteme, *Math. Ann.*, *69*, 331–371, 1910.

Kader, B. A., and A. M. Yaglom, Mean fields and fluctuation moments in unstably stratified turbulent boundary layers, *J. Fluid Mech.*, *212*, 637–662, 1990.

Kader, B. A., and A. M. Yaglom, Spectra and correlation functions of surface layer atmospheric turbulence in unstable thermal stratification, in *Turbulence and Coherent Structures*, edited by O. Metais and M. Lesieur, pp. 387–412, Kluwer Academic, Norwell, Mass., 1991.

Kaimal, J. C., Flux and profile measurements from towers in the boundary layer, in *Probing the Atmospheric Boundary Layer*, edited by D. H. Lenschow, pp. 19–28, American Meteorological Society, Boston, Mass., 1986.

Kaimal, J. C., J. Wyngaard, Y. Izumi, and O. Cote, Spectral characteristics of surface layer turbulence, *Q. J. R. Meteorol. Soc.*, *93*, 305–317, 1972.

Katul, G. G., and M. B. Parlange, A Penman-Brutsaert model for wet surface evaporation, *Water Resour. Res.*, *28*, 121–126, 1992.

Katul, G. G., and M. B. Parlange, On the active role of temperature in surface layer turbulence, *J. Atmos. Sci.*, *51*, 2181–2195, 1994.

Liandrat, J., and F. Moret-Bailly, The wavelet transform: Some applications to fluid dynamics and turbulence, *Eur. J. Mech., B, Fluids*, *9*, 1–19, 1990.

Lumley, J., Interpretation of time spectra measured in high intensity shear flows, *Phys. Fluids*, *6*, 1056–1062, 1965.

Mahrt, L., Eddy asymmetry in the shear heated boundary layer, *J. Atmos. Sci.*, *48*, 472–492, 1991.

Mallat, S., A theory for multiresolution signal decomposition: The wavelet representation, *IEEE Trans. Pattern Anal. Mach. Intell.*, *11*, 674–693, 1989a.

Mallat, S., Multiresolution approximations and wavelet orthonormal bases of $L^2(R)$, *Trans. Am. Math. Soc.*, *315*, 69–87, 1989b.

McBean, G. A., Instrumentation requirements for eddy correlation measurements, *J. Appl. Meteorol.*, *11*, 1078–1084, 1972.

Meneveau, C., Analysis of turbulence in the orthonormal wavelet representation, *J. Fluid Mech.*, *232*, 469–520, 1991a.

Meneveau, C., Dual spectra and mixed energy cascade of turbulence in the wavelet representation, *Phys. Rev. Lett.*, *11*, 1450–1453, 1991b.

Meyer, Y., Orthonormal wavelets, in *Wavelets: Time-Frequency Methods and Phase Space*, edited by J. M. Combes, A. Grossmann, and P. Tchamitchian, pp. 21–37, Springer-Verlag, New York, 1989.

Monin, A. S., and A. M. Yaglom, *Statistical Fluid Mechanics*, vol. II, edited by J. Lumley, 874 pp., MIT Press, Cambridge, Mass., 1975.

Parlange, M. B., and G. G. Katul, An advection-aridity evaporation model, *Water Resour. Res.*, *28*, 127–132, 1992.

Powell, D., and C. E. Elderkin, An investigation of the application of Taylor's hypothesis to atmospheric boundary layer turbulence, *J. Atmos. Sci.*, *31*, 990–1002, 1974.

Press, W. H., B. P. Flannery, S. A. Teukolsky, and W. T. Vetterling, *Numerical Recipes: The Art of Scientific Computing*, 702 pp., Cambridge University Press, New York, 1990.

Tanner, B. D., Use requirements for Bowen Ratio and Eddy Correlation determination of evapotranspiration, paper presented at the 1988 Specialty Conference of the Irrigation and Drainage Division, Am. Soc. Civ. Eng., Lincoln, Neb., 1988.

Taylor, G. I., The spectrum of turbulence, *Proc. R. Soc., A, CLXIV*, 476–490, 1938.

Tennekes, H., and J. Lumley, *A First Course in Turbulence*, 300 pp., MIT Press, Cambridge, Mass., 1972.

Willis, G. E., and J. Deardorff, On the use of Taylor's translation hypothesis for diffusion in the mixed layer, *Q. J. R. Meteorol. Soc.*, *102*, 817–822, 1976.

Wyngaard, J. C., and S. F. Clifford, Taylor's hypothesis and high-frequency turbulence spectra, *J. Atmos. Sci.*, *34*, 922–929, 1977.

Yamada, M., and K. Ohkitani, Orthonormal expansion and its application to turbulence, *Prog. Theor. Phys. Prog. Lett.*, *83*, 819–823, 1990.

Yamada, M., and K. Ohkitani, Orthonormal wavelet analysis of turbulence, *Fluid Dyn. Res.*, *8*, 101–115, 1991a.

Yamada, M., and K. Ohkitani, An identification of energy cascade in turbulence by orthonormal wavelet analysis, *Prog. Theor. Phys.*, *86*, 799–815, 1991b.

G. G. Katul, School of the Environment, Duke University, Durham, NC 27706.

M. B. Parlange, Hydrologic Science, 131 Veihmeyer Hall, University of California, Davis, CA 95616. (e-mail: mbparlange@ucdavis.edu)

(Received July 5, 1994; revised December 14, 1994; accepted December 29, 1994.)